



# Measurement of wind-induced motion of crop canopies from digital video images

Charlotte Py<sup>a,\*</sup>, Emmanuel de Langre<sup>a</sup>, Bruno Moulia<sup>b,1</sup>, Pascal Hémon<sup>a</sup>

<sup>a</sup>*Département de Mécanique, LadHyX, CNRS-École Polytechnique, 91128 Palaiseau, France*

<sup>b</sup>*Unité d'Ecophysiologie des Plantes Fourragères, INRA, 86600 Lusignan, France*

Received 19 July 2004; received in revised form 21 February 2005; accepted 14 March 2005

## Abstract

We present a new measurement technique based on image correlation to capture the wind-induced motions of crop canopies. Tests were carried out on an alfalfa field submitted to natural wind. The motion is video-recorded from the side of the field and we take advantage of the natural periodicity of the crop to correct the distortion due to perspective. The computation of the canopy motions between successive images is based on Particle Image Velocimetry (PIV), and takes advantage of the natural small-scale heterogeneities of the canopy. It provides the two-dimensionnal spatio-temporal velocity field of the crop top surface with high spatial and temporal resolution. The Bi-Orthogonal Decomposition (BOD) of the velocity field then reveals large coherent propagating structures that scale with typical wavelength of wind fluctuation over canopies.

© 2005 Elsevier B.V. All rights reserved.

*Keywords:* Plant motion; Wind; PIV; BOD; Thigmomorphogenesis; Lodging

## 1. Introduction

Interest on wind-induced plant motions has been motivated for a long time by the problems of lodging in crops (permanent displacement of stems from the vertical) and their economic consequences, Baker

(1995). In the last decade, biomechanical studies of crop lodging have been conducted to analyse and model the lodging resistance (e.g. Baker (1995), Farquhar and Meyer-Phillips (2001), Sterling et al. (2003), Berry et al. (2003)). Wind-induced motion has also a direct effect on plant growth in height and diameter, called thigmomorphogenesis (Jaffe, 1973). Recently, biomechanical studies on thigmomorphogenesis (Crook and Ennos (1996), Coutand and Moulia (2000)) has brought new interest in this field of research. In both cases however, a more complete understanding of plant motion would be necessary (Berry et al., 2003).

It has been demonstrated that dynamic loading due to the fluctuation in wind velocity on top of the canopy

\* Corresponding author. Tel.: +33 0 1 69 33 36 75; fax: +33 0 1 69 33 30 30.

*E-mail addresses:* [cpy@ladhyx.polytechnique.fr](mailto:cpy@ladhyx.polytechnique.fr) (C. Py), [delangre@ladhyx.polytechnique.fr](mailto:delangre@ladhyx.polytechnique.fr) (E. de Langre), [moulia@clermont.inra.fr](mailto:moulia@clermont.inra.fr) (B. Moulia), [pascal.hemon@ladhyx.polytechnique.fr](mailto:pascal.hemon@ladhyx.polytechnique.fr) (P. Hémon).

<sup>1</sup> Present address: PIAF, INRA, 234 avenue du Brézat, 63039 Clermont-Ferrand, France.

$c$	phase velocity of the coherent structures of the canopy motion
$d$	distance from the camera to the center of the canopy surface
$E$	total kinetic energy of the canopy motion
$f$	principal temporal frequency of the canopy motion
$g$	grey level signal of the image
$N$	number of spatio-temporal modes considered in the BOD
$N_s$	number of spatial nodes of $U$
$N_t$	number of time steps of $U$
$p_1, p_2$	perspective geometrical transformation
$R$	cross-correlation function
$S$	spatial correlation matrix of $U$
$T$	temporal correlation matrix of $U$
$u, v$	$x$ - and $y$ -components of $U$
$U$	velocity field of the canopy motion
$W_{in}$	interrogation window of an image
$x, y$	coordinates in the image frame of reference
$X, Y$	coordinates in the real plane frame of reference
$\alpha_k$	$k$ th eigenvalue of $T$ and $S$
$\Delta$	principal wavelength of the canopy motion
$\theta$	camera inclination angle
$\lambda_x, \lambda_y$	characteristic visual length scales of the crop image with perspective
$\Lambda$	characteristic visual length scale of the crop
$\mu_k$	$k$ th temporal eigenvector ( <i>chronos</i> )
$\phi_k$	$k$ th spatial eigenvector ( <i>topos</i> )

(wind gusts or sweeps) is much more important to plant motion and momentum transfer than the static loading related to the mean drag (Finnigan, 2000). Such fluctuation of wind over canopies has been widely studied, see Finnigan (2000) for a review. Wind velocity measurements on various canopies have revealed the existence of large coherent structures propagating over the canopy surface, scaling with the height of the canopy. Those structures are created by an instability mechanism similar to that of a mixing

layer (Raupach et al., 1996). They are responsible for a large part of the transfer of momentum to the crop (Finnigan, 1979).

The motion of the canopy itself shows propagating structures that can be seen by the eye (Inoue (1955), Finnigan (1979)), see Fig. 1. Those patches of coherent waving in crops are usually called “honami”, as first introduced by Inoue (1955). Even though the kinematics of single stem oscillations have been studied in some detail ((Flesch and Grant, 1992a,b; Farquhar et al., 2000)), and a few dynamical models proposed (Flesch and Grant (1991), Farquhar et al. (2000), Spatz and Zebrowski (2001), Spatz and Speck (2002), Bruchert et al. (2003)), the global behavior of a canopy under natural wind seems far more complex. Models of the motions of sets of interacting flexible plants in a canopy have been proposed (Doaré et al., 2004) and a preliminar approach of the coupling of wind mixing layer instability with flexible canopy has been developed (Py et al., 2004).

However despite large sets of measurements on wind velocities, no direct measurements of global canopy motion caused by wind have been done. Contact sensors and strain gauges are limited to the measurement of the motion of a few individual plants (Finnigan (1979), (Flesch and Grant, 1992a,b; Sterling et al., 2003)). Moreover, the compliance and lightness of crop plants like wheat at early stages or alfalfa in their vegetative stages make the use of sensors difficult as they may disturb significantly the motion. A non-intrusive method for the measurement of the motion of crop plants would thus be much more adequate. Moreover, to characterise spatio-temporal structures, a large set of adjacent plants in the canopy have to be measured simultaneously with high spatial and temporal resolution. An optical measurement technique therefore appears promising. In fluid dynamics the Particle Image Velocimetry (PIV) technique, based on image correlations, is a very efficient and accurate method to characterise quantitatively spatio-temporal motions (Raffel et al., 1998). This technique was adapted here to measure the motion of a canopy submitted to natural wind.

In this paper the response of the canopy to the wind load is studied quantitatively using video measurements and PIV. Focus is put on the analysis of the spatio-temporal behavior of the motion of a crop exposed to natural wind, and on the detection of

coherent structures of the plants motion. In order to extract such coherent structures from a complex spatio-temporal signal, some signal processing is necessary: Bi-Orthogonal Decomposition (BOD), a now classical technique in aerodynamics, allows to analyse such a signal simultaneously in time and space (Aubry et al. (1991), Hémon and Santi (2003)).

This paper is focused on the technical aspects of the measurement approach. The three steps of the technique, namely the data acquisition, the velocity measurement, and the Bi-Orthogonal Decomposition of the signal are presented respectively in Sections 2 to 4. Each part is illustrated and discussed using preliminary results on the motion of an alfalfa crop under wind. A discussion follows in Section 5.

## 2. Experimental set-up

### 2.1. Raw data acquisition

The observations took place at Lusignan, France (46 ° 28'N, 0 ° 04'E, altitude 150 m) under field conditions, in May 2003. An alfalfa field (*Medicago sativa* L. cv *Mercedes*) was grown under standard agrotechnical procedures. The wind-induced global motion of the crop was recorded under a natural wind of about 3 m s<sup>-1</sup> mean velocity (Fig. 1).

Movies were recorded from the side of the field with a standard digital video camera mounted on a 2.5 m high tripod, Fig. 2. The temporal resolution of the video camera was 25 images per second, and the image size was 400,000 pixels. Each movie was transformed into a sequence of digital images using Adobe Premiere software (Adobe Systems Incorporated). In the treatments, only the grey level of the images was considered, and the images were treated as mathematical matrices. The geometrical distortion due to perspective was batch-corrected on each image of a sequence. The motion measurement was then implemented on the corrected images with a PIV algorithm on Matlab called MatPIV (Sveen, 2000). The spatio-temporal velocity field obtained for each sequence was then analysed using a Bi-Orthogonal Decomposition code (Aubry et al., 1991).

About thirty 10 s sequences of both wheat and alfalfa motion were recorded and analysed. Only a few typical results are presented here to illustrate the technique.

### 2.2. Image distortion rectification

As the movies were recorded from the side of the crop field, the images were distorted by perspective, i.e. the length scales are smaller at the top of the image than at its bottom. This geometric distortion needs to be corrected before exploiting the images, a common feature in optical measurements, see for instance Muste et al. (1999) in large scale PIV. The geometrical transformation due to perspective (given in the Appendix A) only depends on the viewing parameters: the camera inclination  $\theta$  and the distance  $d$  from the camera to the center of the object, in our case the center of the field, see Fig. 2. In practice it is not easy to get a direct measurement of those parameters, particularly  $d$ , in crop field situations. The classical and most recommended technique consists in using a network of regularly spaced targets planted in the field. On the perspective image of the field, measuring the evolution of the distance between targets along two directions from the bottom to the top of the image gives an estimate of  $\theta$  and  $d$  (see Appendix A).

In our case targets could not be planted in the alfalfa field without partly spoiling the crop. The perspective distortion was therefore measured by exploiting the natural regularity of the crop. Indeed in a crop field local characteristic length scales can be found, such as the distance between plants or the width of plants. In conditions of homogeneous soil, light and watering, these length scales can be assumed to be constant all over the field. On a given image any variation of these scales therefore results from perspective effects and can be used to derive the distortion parameters. We used here a characteristic length scale based on the spatial variation of the grey level signal of an image of the crop. More details on this technique are given in the Appendix A.

Once the perspective parameters  $\theta$  and  $d$  were found for one image of a sequence, the correction, namely the inverse geometrical transformation, was applied to each pixel of the image, and this operation was repeated for each consecutive image of the sequence. In the correction operation, the original pixel mesh of the image was transformed into a corrected mesh on which the grey level signal was interpolated. The domain was then restricted to a rectangular shape. A sequence of corrected images, on which the length scales are globally constant, was eventually obtained and used for motion measurement.



Fig. 1. Alfalfa field under wind. Patterns are visible here due to the change in sunlight reflections when plants are bent.

### 3. Motion measurement using a PIV technique

#### 3.1. The PIV technique

The measurement technique proposed to obtain the motion of the crop is optical. It is based on standard

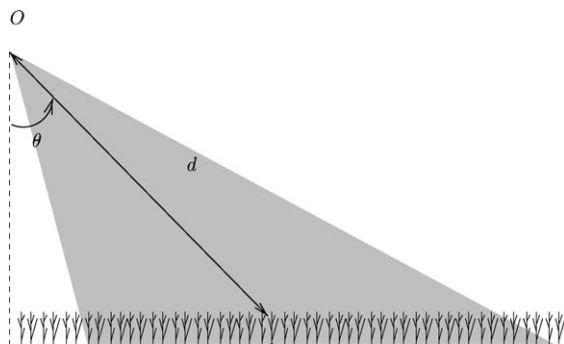


Fig. 2. Camera position  $O$  and inclination  $\theta$  with respect to the field,  $d$  is the distance from the camera to the center of the canopy surface.

Particle Image Velocimetry (PIV) (Raffel et al., 1998), a classical measurement technique in fluid dynamics. This technique has the ability to capture a whole velocity field from two successive frames in a movie sequence. It allows the quantitative identification of spatio-temporal structures even in unsteady flows, as long as the time interval between frames is small in comparison to transition times.

The standard PIV technique in fluid dynamics involves addition of tracer particles to the flow. Illumination in a measurement plane is then provided with a laser sheet, twice within a short time interval. The light scattered by the particles is recorded and digitised. The time interval between consecutive illuminations defines the temporal resolution of the PIV. The PIV image is divided in small subwindows called interrogation windows. The local displacement vector of the tracer particles between the first and second illumination is determined for each interrogation window by means of statistical methods. The amount of match between two local subwindows at

different time steps,  $W_{in_1}$  and  $W_{in_2}$ , is determined through the cross-correlation function, defined as:

$$R(x, y) = \sum_{i=-M/2}^{i=M/2} \sum_{j=-M/2}^{j=M/2} W_{in_1}(i, j) W_{in_2}(i + x, j + y), \quad (1)$$

with adequate normalisation by the standard deviation to get a correlation coefficient. Here,  $i$  and  $j$  denotes pixel numbers, and  $M$  is the size, in pixels, of the interrogation windows. The peak of the cross-correlation function relative to the center of the first interrogation window gives the local displacement between the two illuminations. The velocity is then defined by the displacement divided by the time interval. It is assumed that all particles within one interrogation window have moved homogeneously. The process is then repeated for all interrogation windows of the PIV image. Partially overlapping interrogation windows can be performed in order to increase the spatial resolution.

In this paper we measured the velocity field of the crop surface by applying a modified PIV approach. Contrary to standard PIV applied to fluids, no artificial tracers were used. The crop canopy itself plays the role of particle tracers, the very small scale heterogeneities of the canopy image (i.e. leaves, spikes, ...) allowing to detect local displacements of the crop surface. Additionally no artificial light was needed, as (a) the sun light provides a sufficient level of color signal, (b) it induces sufficient contrast between the different parts of the crop, so that heterogeneities may be detected for image correlation, (c) the plane of measurement is naturally defined by the top of the canopy, provided the crop is dense enough. For correlation computation each image of a movie was divided into small overlapping interrogation windows, with 50% overlap. The optimal size of a subwindow typically scales with the small patterns in the crop, such as a group of a few leaves. The computation of the local displacement vector was performed for each local region between two consecutive images, and this process was repeated for each consecutive image of the movie. Computations were performed using a classical PIV program called MatPIV, Sveen (2000), including standard correction routines (signal to noise ratio, local and global filters, double pass calculation).

For each sequence, the velocity measurement process led to the 2D spatio-temporal velocity field  $U(x, y, t)$  of the crop surface.

### 3.2. Laboratory test case

In order to test the accuracy of the modified PIV technique on the detection of motion of a solid without tracers, a 50 cm square panel of artificial grass was mounted on a moving plate (Fig. 3). The grass fibers' typical length scale,  $\Lambda$ , was here about 1 mm. The plate was driven in an oscillating translation motion by a motor. The displacement of the plate versus time was measured with a laser beam impacting the side of the plate. Simultaneously the motion of the grass panel was recorded with a video-camera situated about 1 m above the panel. We then used the PIV technique described above in order to compute the spatio-temporal velocity field of the grass panel.

As the artificial grass was rigid, the motion of all grass fibers were identical and followed the motion of the panel measured by the laser. Small heterogeneities were added by bending randomly the artificial grass fibers. This allowed a better PIV correlation computation, similar to that of a real crop. The amplitude of displacement of the panel was approximately 1 cm, and the frequency of the motion was varied between 0.5 and 2 Hz. On the movie, this led to displacements of the order of 1 to 4 pixels between consecutive images. The velocity field derived from PIV was found to be uniform and the temporal frequency of oscillation as well as the motion amplitude matched

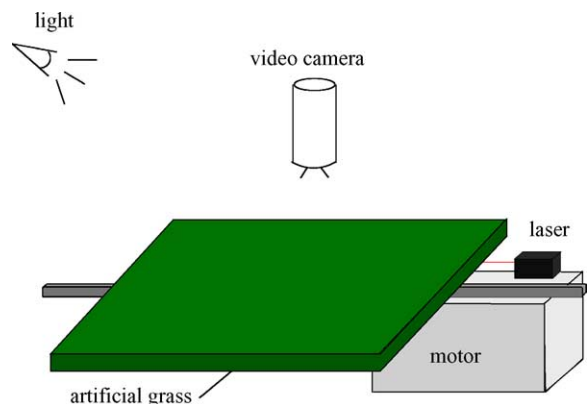


Fig. 3. Scheme of the laboratory test case for the PIV measurement.

the data measured with the laser with less than 5% error (data not shown).

### 3.3. Application to the wind-induced motion of an alfalfa canopy

On a sequence of motion of an alfalfa crop under wind, the velocity field of the canopy surface was computed after perspective correction. The window size was fixed to 44 pixels with 50% overlap. After double-pass calculation, it led to a spatial resolution of 1 value every 11 pixels. The window size was chosen so that the final signal to noise ratio was larger than 1.5, indicating a good accuracy of the correlations calculation. The temporal resolution was that of the video camera, 25 Hz. The CPU time necessary to obtain the crop motion with 2000 points in space and 220 in time ( $\approx 9$  s) was approximately 6 h on a work-station.

Fig. 4 shows a typical velocity field of the alfalfa crop surface at a given time, and Fig. 5 a typical temporal evolution of the two velocity components at a given point. Both spatial and temporal evolutions of the crop motion were detected with sufficient resolution: large structures can be seen in Fig. 4 and well defined oscillations in Fig. 5.

It may be noted that in the upper part of the images (Fig. 4) the computed velocities are found to be smaller than in the rest of the image: the standard deviations of  $u$  and  $v$  are in average 30% smaller in the

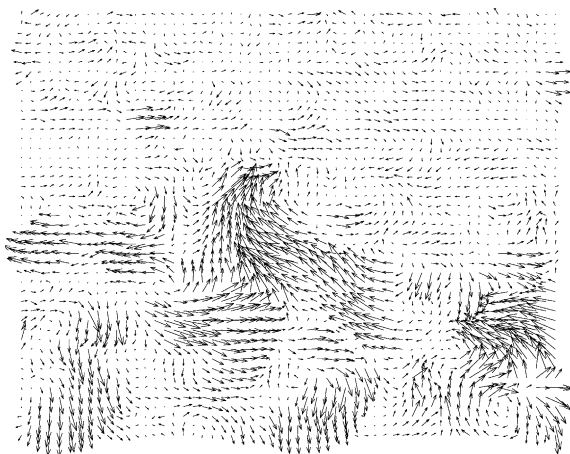


Fig. 4. Instantaneous velocity field of the alfalfa crop. Scale of velocities: maximum velocity is here  $0.2 \text{ m s}^{-1}$ . The mesh increment is  $\Delta_x = \Delta_y = 5 \text{ cm}$ .

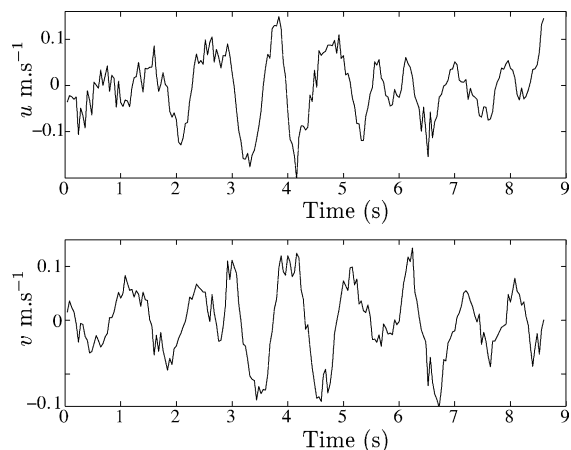


Fig. 5. Temporal evolution of the velocity components  $u$  and  $v$  at a point in the middle of the field shown Fig. 4.

upper fourth of the image. This is due to the fact that these points correspond to crop elements far from the camera, so that the amplitudes of motions are barely perceptible in this part of the image despite perspective correction.

## 4. Bi-Orthogonal Decomposition of the velocity field

The crop velocity field has a complex and rich spatio-temporal behavior. Therefore a specific signal processing is needed to extract the spatio-temporal features.

### 4.1. Theoretical background of Bi-Orthogonal Decomposition

In order to extract the main features of the motion of the plants, we used the Bi-Orthogonal Decomposition (BOD) of the velocity field as initially proposed by Aubry et al. (1991). The principle of the BOD is to carry out a decomposition of a signal depending of space and time in a finite series of spatio-temporal structures. We consider here the velocity field of the motion of the crop surface

$$U(M, t) = \begin{bmatrix} u(M, t) \\ v(M, t) \end{bmatrix}, \quad (2)$$

where  $M$  is the point of coordinate  $(x, y)$ ,  $t$  is time and  $u, v$  are the components of the velocity in the  $x$  and  $y$

directions. The corresponding BOD reads

$$U(M, t) = \sum_{k=1}^{\infty} \sqrt{\alpha_k} \mu_k(t) \Psi_k(M). \quad (3)$$

where  $\Psi_k$  are the spatial functions, referred to as *topos* and  $\mu_k$  are the temporal functions, referred to as *chronos*. Each forms a set of orthogonal functions and the weight factor of each of these spatio-temporal structures ( $\Psi_k, \mu_k$ ) is the real scalar value  $\sqrt{\alpha_k}$ . Aubry et al. (1991) have shown that (i) this decomposition is unique, (ii) the *topos* are the eigenfunctions of the spatial correlation operator of  $U$  with eigenvalues  $\alpha_k$ , (iii) the *chronos* are the eigenfunctions of the temporal correlation operator of  $U$  with the same eigenvalues  $\alpha_k$ , (iv) this series converges in norm, thus allowing truncation to the first  $N$  terms of the series. A remarkable feature of BOD is that the eigenvalues  $\alpha_k$  are common to the spatial eigenfunctions (*topos*) and the temporal eigenfunctions *chronos*. This results from the properties of the spatial and temporal correlation operators which are adjoint.

In practice the signal to be analysed is given in a discrete form which implies that in the above formulation, functions must be replaced by vectors and correlation operators by correlation matrices. Note that the signal is actually a measurable signal, meaning that it is square-integrable, or in other words that all the terms of the correlation matrices have a finite value. In our context, the temporal correlation matrix is defined by

$$T_{ij} = \sum_{p=1}^{N_s} u(M_p, t_i)u(M_p, t_j) + v(M_p, t_i)v(M_p, t_j) + u(M_p, t_i)v(M_p, t_j) + u(M_p, t_j)v(M_p, t_i), \quad (4)$$

where  $N_s$  is the number of spatial nodes of the signal. Similarly the spatial correlation matrix is

$$S = \begin{bmatrix} [S^{uu}] & [S^{uv}] \\ [S^{vu}] & [S^{vv}] \end{bmatrix} \quad (5)$$

where  $S^{ab}$  denotes the correlation matrix with

$$S_{ij}^{ab} = \sum_{q=1}^{N_t} a(M_i, t_q)b(M_j, t_q) \quad (6)$$

with  $N_t$  the number of time steps and  $(ab)$  takes the values of  $(uu)$ ,  $(uv)$ ,  $(vu)$  and  $(vv)$ . The components of

$T$  and  $S$  were normalised by the total kinetic energy of the signal and are therefore rightfully called correlations. Note that here the signal to analyse is two-dimensional in space. The correlation calculation thus takes into account the bidimensionality of the problem, i.e. correlations between the  $x$  and  $y$  components of  $U$ , namely  $u$  and  $v$ .

For this application the number of time steps  $N_t$  will be smaller than the number of spatial nodes  $N_s$ . Hence the dimension of  $T$  which, is  $N_t^2$ , will be smaller than that of  $S$ , which is  $4N_s^2$ . As the eigenvalues of  $T$  are also eigenvalues of  $S$ , it is thus more convenient in terms of computing time to solve first the temporal eigenvalue problem and to deduce afterwards the spatial modes. The *chronos* (temporal eigenfunctions) were thus computed first by solving the discretised eigenvalue problem:

$$T\mu = \alpha\mu, \quad (7)$$

where  $T$  has dimension  $N_t^2$  and  $\mu$  has dimension  $N_t$ . The *topos* (spatial eigenfunctions) were then derived using the projection of Eq. (3) on the set of *chronos*,

$$\Psi_k(M) = \frac{1}{\sqrt{\alpha_k}} \sum_{i=1}^{N_t} U(M, t_i)\mu_k(t_i). \quad (8)$$

Note that this projection using the original signal  $U$ , based on the orthogonality property of BOD, does not alter the phase information of the signals.

In the decomposition of Eq. (3), the spatio-temporal modes  $(\mu_k, \Psi_k)$  may be ranked in decreasing order of their contribution in the total kinetic energy. The eigenvalue  $\alpha_k$  represents the kinetic energy of the  $k^{th}$  spatio-temporal mode (Hémon and Santi, 2003). The rate of convergence of the decomposition series is a test of the presence of large coherent structures. With a good convergence rate the first sets of *chronos* and *topos* contain most of the space and time characteristics of the motion.

The BOD bears some relation with the more classical Karhunen-Loève decompositions, such as the Principal Component Analysis (PCA), the Singular Value Decomposition (SVD), the Empirical Orthogonal Functions (EOF), or the Proper Orthogonal Decomposition (POD), see for instance Moin and Moser (1989), Finnigan and Shaw (2000). Yet a major difference exists, which has significant practical consequences in the present case : the BOD technique

does not require the signal to satisfy any particular assumption (other than being square-integrable, which is the case of all measurable signals). It can therefore be used with non-stationary signals, even showing intermittent events, which is the case here with crop motion under natural wind. In particular, the assumption of ergodicity, i.e. the temporal average being identical to the spatial average, is unnecessary with the BOD, while the Karhunen-Loève decompositions such as POD or EOF require it. Furthermore, POD or EOF formally require that the individual samples of the signal have a Gaussian distribution (Marriot, 1974) although they are often used without checking this particular feature, as pointed out by Hémon and Santi (2003). Eventually the most important difference of BOD is certainly the real simultaneous analysis in both space and time that is provided, as here the relative phase information is not lost. BOD can thus provide not only the extraction of the coherent structures of the signal but also the description of how these coherent structures evolve or are convected.

In terms of physical interpretation, the spatial and temporal eigenvectors, when ordered in decreasing level of kinetic energy, characterize the main spatio-temporal components of a given evolution of the crop velocity field and their relative contribution. As is illustrated further, this is particularly useful for the purpose of extracting the size and phase velocity of

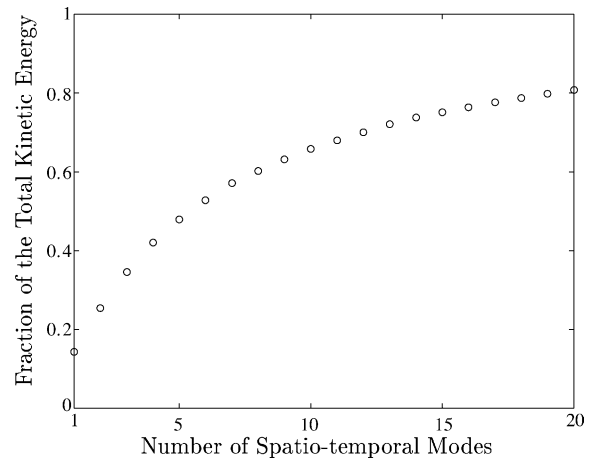


Fig. 6. Fraction of the total kinetic energy recovered versus number of spatio-temporal modes considered in the Bi-Orthogonal Decomposition.

convected patterns that may exist in the motion of the canopy.

#### 4.2. BOD analysis of the crop motion

BOD was applied to the spatio-temporal velocity field  $U(x, y, t)$  describing the motion of an alfalfa field obtained in Section 3.3. Fig. 6 shows the cumulated energy recovered from the signal BOD as a function of the number of spatio-temporal modes considered. It

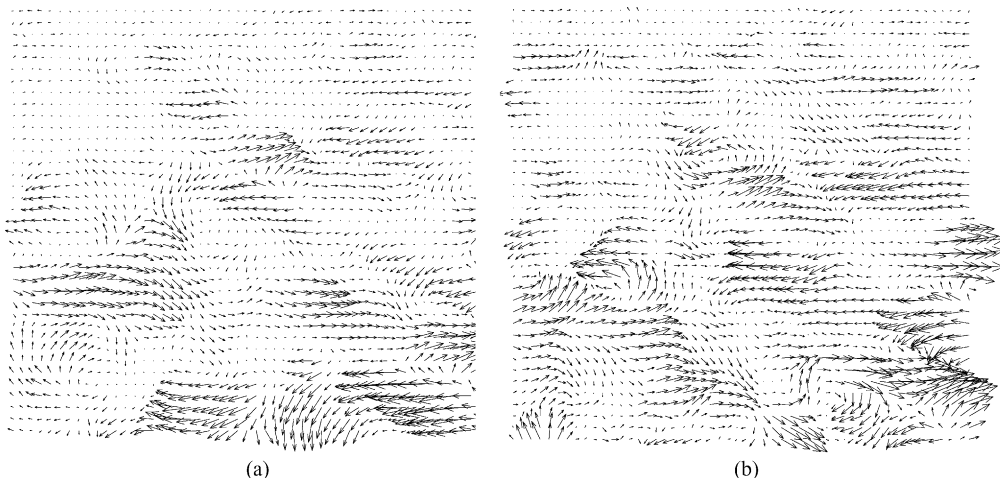


Fig. 7. First (a) and second (b) *topos* (spatial eigenvector) of the bi-orthogonal decomposition of the motion of an alfalfa crop. The amplitude is arbitrarily scaled.

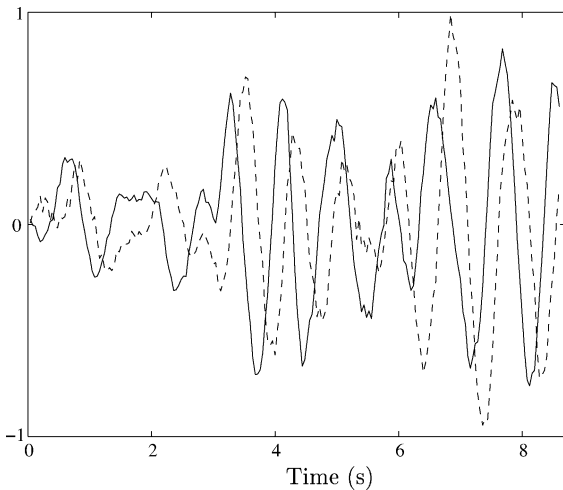


Fig. 8. First (—) and second (- -) *chronos* (temporal eigenvector) of the Bi-Orthogonal Decomposition of the motion of an alfalfa crop. The amplitude is arbitrarily scaled.

was normalised by the total kinetic energy of  $U$ , namely  $E = \sum_{i=1}^N T_{ii}$ . The plot of the cumulated energy illustrates the convergence of the BOD. When considering only fifteen *chronos-topos* couples of the decomposition, more than 75% of the total kinetic energy was recovered. This shows a good convergence of the BOD and indicates the coherence of the motion of the crop surface. The entropy of the velocity field may also be computed, see Hémon and

Santi (2003). If the entropy is close to zero, the signal is totally determined, and all its energy is concentrated in the first terms of the BOD. This would be the case of a solid body motion. Conversely when the entropy is close to one, the signal is highly disordered, and a large number of modes is necessary to recover the signal. For instance, the BOD of a homogeneous noise is reduced to a Fourier Decomposition with an infinitely slow convergence rate. In the particular case presented here, the entropy reached 0.7, which is rather high. The level of entropy of the signal associated to the good convergence rate of the decomposition highlights the interest of the BOD: the signal to study is here highly disordered but contains a coherent part, and the decomposition allows extraction of the coherent motion from the noise.

Let us focus on the two most energetic spatio-temporal modes of the decomposition. Fig. 7a and b show the spatial eigenvectors (*topos*) of modes number 1 and 2, and Fig. 8 their associated temporal eigenvector (*chronos*). Note that *topos* and *chronos* are eigenvectors and are therefore shown here with arbitrary amplitude. The *topos* vector fields are composed of large-scale organised motions. We may decompose those vector fields into their invariants: divergence and curl. The curl fields of *topos* 1 and 2, Fig. 9a and b, permits identification more precisely of these coherent structures. In both

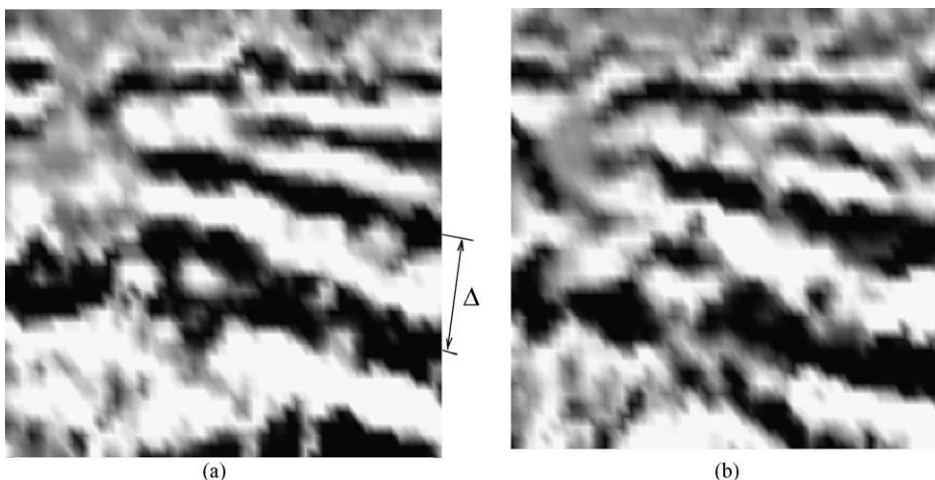


Fig. 9. Curl of the first (a) and second (b) *topos* (spatial eigenvector). White stands for clockwise curl and black for counter-clockwise curl. The arrow represents a typical wavelength  $\Delta$  of the coherent structures.

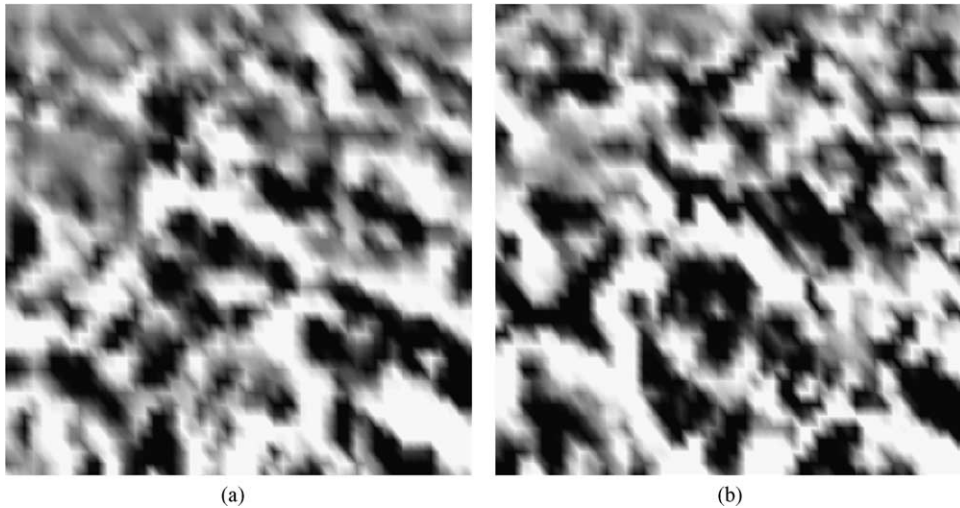


Fig. 10. Divergence of the first (a) and second (b) *topos* (spatial eigenvector). White stands for positive divergence, and black for negative divergence.

fields, those structures appeared as large parallel stripes. The corresponding typical length scale  $\Delta$  was approximately 1 m. This is of the same order of magnitude as the size of the coherent structures in the wind itself, as observed by Finnigan (2000) over similar canopies. A more detailed analysis of the *topos* (spatial eigenvectors) showed that there is a phase lag in space between the two curl fields associated with *topos* 1 and 2. The divergence fields of the same *topos*, Fig. 10a and b, also show patterns but less emphasized and without the directionnal anisotropy of the curl field.

The *chronos* (temporal eigenvectors) 1 and 2 (Fig. 8) have a regular oscillating behavior. A Fourier analysis reveals that they have a common and well defined frequency  $f$  of about 1.2 Hz. This frequency is typical of free vibration of alfalfa stems of these heights (Doaré et al., 2004). It is remarkable that the BOD allows to extract a dominant temporal frequency, whereas it was impossible to detect one by eye on the original recorded motion.

It should also be noted that those two *chronos* were phase-lagged in time. This feature, associated with the phase-lagged spatial structures of the *topos* 1 and 2,

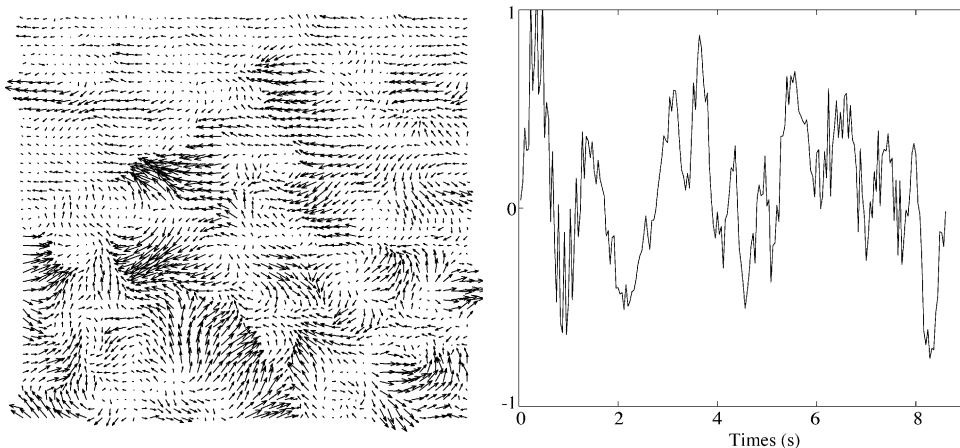


Fig. 11. Spatio-temporal mode number 15: *topos* and associated *chronos*. The amplitudes are arbitrarily scaled.



Fig. 12. Curl of the *topos* (spatial eigenvector) number 15.

indicates that the simple combination of these first two spatio-temporal modes results in propagating patterns. The corresponding phase velocity  $c = f\Delta$  would be of the order of  $1.2 \text{ m s}^{-1}$ .

The next spatio-temporal modes in the BOD series (3, 4, ...) display similar features, namely large coherent structures for the *topos*, pairing of the *chronos*, and propagation properties with the same temporal frequency as the most energetic *chronos*. Only the less energetic modes involved decorrelated motions with much smaller scales. A typical example is shown with mode 15 on Fig. 11. The corresponding curl field, Fig. 12, displays smaller structures.

## 5. Discussion

Although illustrated here on the motion of an alfalfa crop, this approach can easily be extended to various canopy dynamics. It was applied to several other movies of alfalfa motion under various wind conditions and also tested on a wheat field (data not shown). In most cases the technique allowed to detect large coherent propagating structures. The temporal and spatial resolution of a standard video-camera were found sufficient for all these measurements. Note that the signal processing part of this approach (distortion correction, PIV and BOD) requires significant CPU time, typically 1 h for 1 s of real time.

We now discuss in more detail each step of the proposed approach. In terms of recording parameters, the capture of the motion of the plants, as well as the perspective correction, are more accurate when the viewing angle  $\theta$  is small. With a large  $\theta$ , the image is greatly deformed by perspective, leading to the creation of a lot of noise in the interpolation of the image on the new pixel mesh. Moreover the motion of the plants situated at the top of the initial image are barely perceptible. Conversely the drawback of a small viewing angle is that it reduces the area of crop field visible with the video-camera. Clearly a higher position of the camera, allowing for a larger scene with small viewing angle, would be preferable. Specific aspects of the distortion correction are discussed in the [Appendix A](#).

The derivation of the plants motion is based on advanced image correlation: the PIV technique includes additional filtering thus yielding more accurate data. This is an important feature as the crop velocity field is to be analysed in terms of spatio-temporal structures. Note also that in the PIV process the choice of the subwindow size is important. It should be small enough so that globally all pixels of a subwindow follow the same displacement during the time interval considered, and large enough so that in a given subwindow the plant parts lying under the crop surface represent a minor proportion of the whole subwindow area. Concerning the percentage of overlap between subwindows, a higher percentage allows to increase the spatial resolution but introduces artificial correlation in the resulting velocity field. A 50% overlap is a usual compromise in standard PIV and was found suitable here. The motion measurement using PIV can easily be applied to other canopies of various scales, from grass to forest canopies. It would not be accurate on a sparse canopy because in this case a unique measurement plane can not be defined. Each small region of the image of a sparse canopy is indeed composed of plant parts at different heights and the results of the correlation technique in the PIV cannot be associated with velocities of a plane.

The next step of the approach is the BOD analysis. BOD is of particular interest in the analysis of the crop velocity field since this signal is highly disordered but contains a coherent part. BOD allows to extract the spatio-temporal coherent structures of the motion and also provides their propagation properties. This important characteristic results from the simulta-

neous time and space decomposition of BOD. The coherence of the motion appears more clearly in the curl of the *topos* (spatial eigenvectors) than in their divergence. This unexpected feature might lead to interesting information on the complex coupling between the wind dynamics and the motion of the crop. The temporal frequency recovered from the first *chronos* (temporal eigenvectors) of the decomposition is close to the free oscillation frequency of alfalfa (Doaré et al., 2004). This indicates that plants interactions in this crop is probably rather low.

## 6. Concluding remarks

The experimental approach proposed here consists of a set of several independent techniques: (i) video-recording of the canopy motion with distortion correction based on the crop homogeneity, (ii) PIV derivation of the motion, and (iii) BOD analysis of the velocity field to identify the spatio-temporal propagating structures. The technique is easy to implement, portable and low-cost, requiring only standard material and signal processing. It can therefore be easily applied to a large variety of canopies. This is today the only simple approach to derive in-situ characteristics of the motion of whole canopies under wind. The preliminary results shown in this paper on an alfalfa field are promising and a systematic set of measurements on several crops is currently being done. This should allow to derive two kinds of information:

- the level and frequency of solicitations perceived by the plants for a given mean wind velocity. This is of primary importance for thigmomorphogenic (Coutand and Mouliat, 2000) and lodging analyses (Baker, 1995).
- the relation between the characteristics of the propagating structures on the canopy and that of the propagating structures in the wind field as already measured by other techniques (Finnigan, 2000). This should provide a better insight into the mechanisms of transfer of momentum from the fluid to the canopy through coherent structures, and allow to assess the validity of current models such as Py et al. (2004).

## Acknowledgements

The authors acknowledge the precious contribution of Dr. Didier Combes, from INRA-UEPF, to the experimental campaign and also thank Dr. Yves Brunet, from INRA-EPHYSE, and Dr. Olivier Doaré, from ENSTA, for very helpful discussions and advice.

## Appendix A. Perspective transformation correction

We recall here classical results on perspective projection. Seen from the camera, point  $O$ , Fig. A.1a, a

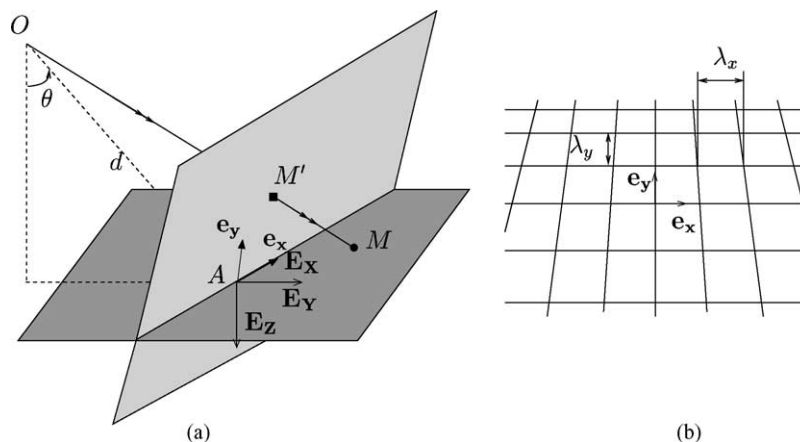


Fig. A.1. (a) Real plane (canopy) in dark grey, image plane in light grey (perpendicular to the  $OA$  axis), and camera position  $O$ . (b) A regular grid of length scale  $\Lambda$  on the real plane is projected on the image plane into a distorted grid with length scales  $\lambda_x$  and  $\lambda_y$  decreasing with  $y$ .

point  $M(X, Y, 0)$  lying on the canopy plane, is projected on the image plane in  $M'(X', Y', Z')$ . The image plane is defined by  $O, M$ , and  $M'$  being aligned and  $AM'$  being orthogonal to  $OA$ , where  $A$  is the center of the image. This leads to

$$\begin{aligned} X' &= \frac{Xd}{Y\sin\theta + d}, & Y' &= \frac{Yd\cos^2\theta}{Y\sin\theta + d}, \\ Z' &= \frac{-Yd\sin\theta\cos\theta}{Y\sin\theta + d} \end{aligned} \tag{A.1}$$

In the frame of reference of the image plane ( $A, e_x, e_y$ ), the coordinates of  $M'$  are

$$x = \frac{Xd}{Y\sin\theta + d}, \quad y = \frac{Yd\cos\theta}{Y\sin\theta + d} \tag{A.2}$$

and therefore the perspective transformation reads  $x = p_1(X, Y), y = p_2(Y)$ .

Using classical continuum kinematics, see for instance Salençon (2001), we may express the transformation of a characteristic length  $\Lambda_X$  along  $E_X$  (resp.  $\Lambda_Y$  along  $E_Y$ ) on the canopy plane, into  $\lambda_x$  (resp.  $\lambda_y$ ) on the image plane as follows

$$\lambda_x^2 = \Lambda_X^2 \left( \frac{\partial p_1}{\partial X} \right)^2, \quad \lambda_y^2 = \Lambda_Y^2 \left( \left( \frac{\partial p_1}{\partial Y} \right)^2 + \left( \frac{\partial p_2}{\partial Y} \right)^2 \right) \tag{A.3}$$

which leads here to

$$\lambda_x = \Lambda_X \left( 1 - \frac{\tan\theta}{d} y \right), \quad \lambda_y = \Lambda_Y \cos\theta \left( 1 - \frac{\tan\theta}{d} y \right), \tag{A.4}$$

where  $\lambda_y$  is here expressed on the  $x = 0$  line. Measuring on a perspective image the evolutions along  $y$  of two length scales  $\lambda_x$  and  $\lambda_y$ , that are the transforms of respectively  $\Lambda_X$  and  $\Lambda_Y$  on the real plane, allows to identify  $\theta$  and  $d$ . In practice, a network of regularly spaced targets planted in the crop can play the role of a regular mesh, see Fig. A.1b. Here, we use as a reference the natural regularity of a crop. The natural characteristic length scale of a crop, such as the width of the plants or the distance between plants, appear as a wavelength in the spatial evolution of the grey level signal  $g$  of an image of the crop. We define here such a wavelength by a

simple central frequency formula, as follows

$$\lambda = 2\pi \frac{\langle g \rangle_l}{\langle \partial g / \partial s \rangle_l}, \tag{A.5}$$

where  $s$  is the coordinate along the line and  $\langle \rangle$  denotes the standard deviation along the line  $l$ . By considering lines parallel to the  $x$ -axis (resp.  $y$ -axis) the length scales  $\lambda_x$  (resp.  $\lambda_y$ ) may thus be estimated as well as their evolution versus  $y$  by varying the  $y$ -position of the line  $l$ . We now assume that these  $\lambda_x(y)$  and  $\lambda_y(y)$  dependances follow Eq. (A.4), being the geometrical transformations of a unique  $\Lambda = \Lambda_X = \Lambda_Y$  length scale, as the crop is assumed to be isotropic. The parameters  $\Lambda, \theta$  and  $d$ , may be then estimated by linear fits of  $\lambda_x$  and  $\sqrt{\lambda_y}$  versus  $y$ .

This image distortion correction procedure based on the measurement of the characteristic length scale of the crop image offers the advantage of being portable. It does not require preliminary planting of reference targets in the field, in such a way that any part of a crop can be filmed without specific preparation. Despite this advantage, the correction procedure has important limits. It requires a visually homogeneous crop and homogeneous light conditions when filming. If it is not the case, the grey level signal of the crop image is perturbed by larger scales such as the effect of an inhomogeneous reflected light on the plants leaves, and the length scale  $\lambda$  computed with Eq. (A.5) does not only match the distance between plants but also contains traces of larger wavelengths present in the signal. This leads to discrepancies in the estimation of the perspective distortion. Note also that the present correction procedure, based on three parameters only ( $\theta, d, \Lambda$ ) does not allow correction of the distortion due to the lens aberrations, here estimated to be less than 5 pixels.

## References

- Aubry, N., Guyonnet, R., Lima, R., 1991. Spatiotemporal analysis of complex signals: theory and applications. *J. stat. Phys.* 64, 683–739.
- Baker, C.J., 1995. The development of a theoretical model for the windthrow of plants. *J. Theor. Biol.* 175, 355–372.
- Berry, P.M., Sterling, M., Baker, C.J., Spink, J., Sparkes, D.L., 2003. A calibrated model of wheat lodging compared with field measurements. *Agric. Forest Meteorol.* 119, 167–180.

- Bruchert, F., Speck, O., Spatz, H.C., 2003. Oscillations of plants' stems and their damping: theory and experimentation. *Philos. Trans. R. Soc. Lond. Series B Biol. Sci.* 358 (1437), 1487–1492.
- Coutand, C., Moulia, B., 2000. Biomechanical study of the effect of a controlled bending on tomato stem elongation: local strain sensing and spatial integration of the signal. *J. Exp. Bot.* 51 (352), 1825–1842.
- Crook, M.J., Ennos, A.R., 1996. Mechanical differences between free-standing and supported wheat plants, *Triticum aestivum* L. *Annal. Bot.* 77 (3), 197–202.
- Doaré, O., Moulia, B., de Langre, E., 2004. Effect of plant interaction on wind-induced crop motion. *Transactions of the ASME. J. Biomech. Eng.* 126, 146–151.
- Farquhar, T., Wood, J.Z., van Beem, J., 2000. The kinematics of a wheat struck by a wind gust. *Transactions of the ASME. J. Appl. Mech.* 67, 496–502.
- Farquhar, T., Meyer-Phillips, H., 2001. Relative safety factors against global buckling, anchorage rotation, and tissue rupture in wheat. *J. Theor. Biol.* 211 (1), 55–65.
- Flesch, T.K., Grant, R.H., 1991. The translation of turbulent wind energy to individual corn plant motion during senescence. *Boundary Layer Meteorol.* 55, 161–177.
- Flesch, T.K., Grant, R.H., 1992. Corn motion in the wind during senescence: I. Motion characteristics. *Agron. J.* 84, 748–751.
- Flesch, T.K., Grant, R.H., 1992. Corn motion in the wind during senescence: II. Effect of dynamic plant characteristics. *Agron. J.* 84, 742–747.
- Finnigan, J.J., 1979. Turbulence in waving wheat. I. Mean statistics and honami. *Boundary-Layer Meteorol.* 16, 181–211.
- Finnigan, J.J., 2000. Turbulence in plant canopies. *Annu. Rev. Fluid Mech.* 32, 519–571.
- Finnigan, J.J., Shaw, R.H., 2000. A wind-tunnel study of airflow in waving wheat: an EOF analysis of the structure of the large-eddy motion. *Boundary Layer Meteorol.* 96, 211–255.
- Hémon, P., Santi, F., 2003. Applications of biorthogonal decompositions in fluid-structure interactions. *J. Fluids Struct.* 17, 1123–1143.
- Inoue, E., 1955. Studies of the phenomena of waving plants ("HONAMI") caused by wind. Part 1. Mechanism and characteristics of waving plants phenomena. *J. Agricult. Meteorol. (Japan)* 11, 71–82.
- Jaffe, M., 1973. Thigmomorphogenesis: the response of plant growth and development to mechanical stimulation, with special reference to *Bryonia dioica*. *Planta* 114, 143–157.
- Marriot, F.H.C., 1974. *The Interpretation of Multiple Observations*. Academic Press, London.
- Moin, P., Moser, R.D., 1989. Characteristic-eddy decomposition of turbulence in a channel. *J. Fluid Mech.* 200, 451–509.
- Muste M., Xiong Z., Kruger A., Fujita I., 1999. Error estimation in PIV applied to large-scale flows. In: Adrian A., Hassan Y., Meinhart C (Eds.). *Proceedings of the third International Workshop on PIV*.
- Py, C., de Langre, E., Moulia, B., 2004. The mixing layer instability of wind over a flexible crop canopy. *Comptes-Rendus Mécanique* 332, 613–618.
- Raffel, M., Willert, C.E., Kompenhans, J., 1998. *Particle Image Velocimetry: A Practical Guide*, third ed. Springer-Verlag, Berlin.
- Raupach, M.R., Finnigan, J.J., Brunet, Y., 1996. Coherent eddies and turbulence in vegetation canopies: the mixing layer analogy. *Boundary-Layer Meteorol.* 78, 351–382.
- Salençon, J., 2001. *Handbook of Continuum Mechanics*. Springer.
- Spatz, H.C., Speck, O., 2002. Oscillation frequencies of tapered plant stems. *Am. J. Bot.* 89 (1), 1–11.
- Spatz, H.C., Zebrowski, J., 2001. Oscillation frequencies of plant stems with apical loads. *Planta* 214, 215–219.
- Sterling, M., Baker, C.J., Berry, P.M., Wade, A., 2003. An experimental investigation of the lodging of wheat. *Agricult. Forest Meteorol.* 119, 149–165.
- Sveen J.K., 2000. An Introduction to MatPIV 1.4, Internet Publication. <http://www.math.uio.no/jks/matpiv/index.html>.